論文 / 著書情報
Article / Book Information

題目(和文)	
Title(English)	Formation mechanism of dislocation cell structures during fatigue in multiple-slip-oriented copper single crystals
著者(和文)	WANGBohan
Author(English)	Bohan Wang
出典(和文)	学位:博士(工学), 学位授与機関:東京工業大学, 報告番号:甲第12871号, 授与年月日:2024年9月20日, 学位の種別:課程博士, 審査員:藤居 俊之,小林 覚,村石 信二,小林 郁夫,LEI XIAOWEN
Citation(English)	Degree:Doctor (Engineering), Conferring organization: Tokyo Institute of Technology, Report number:甲第12871号, Conferred date:2024/9/20, Degree Type:Course doctor, Examiner:,,,,
学位種別(和文)	博士論文
Category(English)	Doctoral Thesis
種別(和文)	要約
Type(English)	Outline

（博士課程）
Doctoral Program

論 文 要 約

THESIS OUTLINE

系・コース： Department of, Graduate major in	材料 材料	系 コース	
学生氏名： Student's Name	WANG Bohan		

申請学位（専攻分野）： Academic Degree Requested	博士 Doctor of （ 工学 ）
指導教員（主）： Academic Supervisor(main)	藤居 俊之
指導教員（副）： Academic Supervisor(sub)	小林 覺

Formation mechanism of dislocation cell structures during fatigue in multiple-slip-oriented copper single crystals

Fatigue is a phenomenon in which the properties of metals deteriorate under cyclic stress or strain, ultimately leading to failure. Fatigue failure is a major cause of structural damage in a wide range of industries. Fatigue crack initiation and propagation are critical stages prior to fatigue failure. The dislocation cell structures have been shown to have a major influence on the fatigue crack initiation and propagation. Therefore, investigating the formation and evolution of cell structures is essential to gain insight into the fatigue process. However, the studies on the cell structures of multiple-slip-oriented copper single crystals are still insufficient. This thesis conducts fatigue tests on the [001], [011], and [$\bar{1}$11] multiple-slip-oriented copper single crystals to systematically investigate the formation and development of cell structures.

Chapter 1. General introduction

This chapter systematically summarizes the relationship between the cyclic deformation behavior and the orientations of the stress axis in fcc single crystals. In addition, the objectives and results of this study are briefly introduced.

Chapter 2. Characterization of dislocation microstructures in near-[$\bar{1}11$] single crystal copper using high-voltage scanning transmission electron microscopy

In this chapter, fatigue tests of near-[$\bar{1}11$]-oriented copper single crystals were conducted at different constant plastic strain amplitudes (γ_{pl}: $2 \times 10^{-4} \sim 2 \times 10^{-3}$) at room temperature. The dislocation structural characteristics were investigated by high-voltage scanning transmission electron microscopy (HV-STEM).

As shown in Fig.1, at low strain amplitudes ($\gamma_{pl} = 2 \times 10^{-4}$ and 5×10^{-4}), the dislocation structure is a vein-like structure. As the strain amplitude increases ($\gamma_{pl} \geq 1 \times 10^{-3}$), the dislocation structures evolve to two phases consisting of cell bands (CBs) and matrix wall structure. The formation plane of matrix vein-like and wall structures is parallel to the ($\bar{1}11$) plane, which is normal to the sum of the Burgers vectors of dislocations for primary, coplanar, and conjugate slip systems. This mechanism provides a geometrical understanding of the formation process of the ($\bar{1}11$) walls. As shown in Fig.1 (c-f), three types of CBs (parallel to (121), ($\bar{1}\bar{1}2$), and ($\bar{2}1\bar{1}$)) formed inside the two types of deformation bands (($\bar{1}\bar{1}1$) DB I and ($\bar{2}11$) DB II). There is no strict one-to-one correspondence between the formation plane of CB and DB. The state of CB development affected the softening rate of the fatigued specimens. And a positive linear relationship was observed between the shear stress amplitude and the reciprocal of the cell width. The cell width decreased with increasing shear stress amplitude and was independent of the types of CBs.

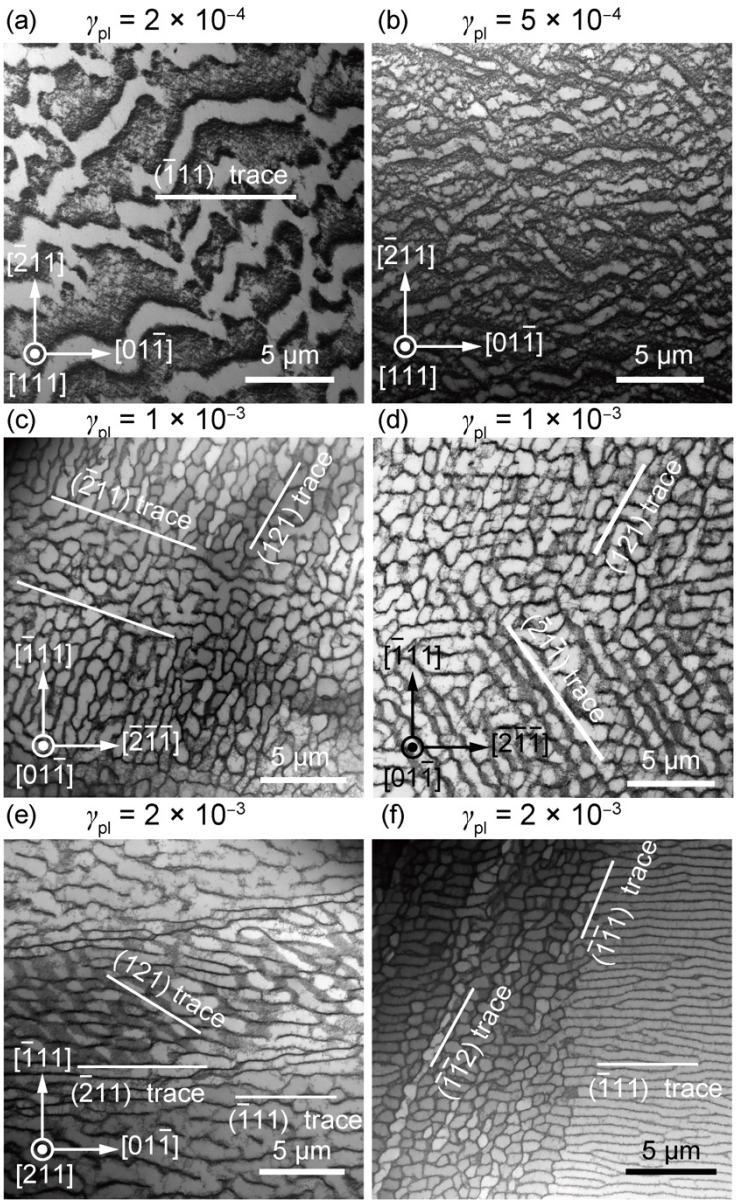

Fig. 1. HV-STEM images of near-[$\bar{1}$11] copper single crystals under (a) $\gamma_{pl} = 2 \times 10^{-4}$, (b) $\gamma_{pl} = 5 \times 10^{-4}$, (c, d) $\gamma_{pl} = 1 \times 10^{-3}$, and (e, f) $\gamma_{pl} = 2 \times 10^{-3}$. (c) and (d) different region of a same specimen. (e) and (f) different specimens.

Chapter 3. Formation mechanism of dislocation network of cell structure in cyclically deformed near-[$\bar{1}$11] copper single crystals

In Chapter 3, the dislocation structures in near-[$\bar{1}$11] copper single crystals were observed by scanning electron microscopy electron-channeling contrast (SEM-ECC) and HV-STEM. The virtual-STEM technique was used to assist in the Burgers vector analysis of the dislocation composition at the (111) cell boundary.

The dislocation structures of the near-[$\bar{1}$11] single crystal copper under $\gamma_{pl} = 2 \times 10^{-3}$ is illustrated in Fig. 2(a). The dislocation network was formed in the channels between the ($\bar{1}$11) dislocation walls. In Fig. 2(a), the red and white areas indicate regions of low- and high-dislocation-density, respectively. The dislocation network formed the early stage of the cell boundary. Upon comparing Fig. 2(b) and (c), the dislocation network gradually became denser and more homogeneous in size as the dislocation density increased. The cell boundary parallel to the (111) primary slip plane was formed by the dislocation networks consisting of multiple types of dislocations. As the dislocation density increased, the dislocations forming the dislocation network underwent transformations. The low-dislocation-density networks, comprising three perfect screw dislocations (**b** = $a/2[\bar{1}01]$, $a/2[\bar{1}10]$, and $a/2[01\bar{1}]$), were formed by the interaction between the primary and coplanar slip systems. In the high-dislocation-density networks, the perfect dislocations and Shockley partial dislocations (**b** = $a/6[11\bar{2}]$, $a/6[2\bar{1}\bar{1}]$, and $a/6[\bar{1}2\bar{1}]$) coexisted, primarily because of the increased dislocation density, which influenced the dislocation dissociation to reduce the elastic energy.

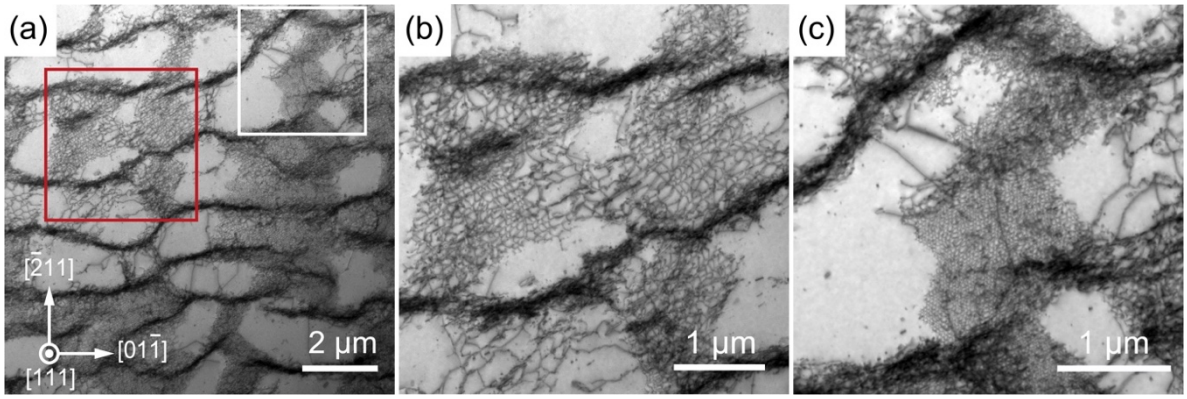

Fig. 2. HV-STEM images of dislocation structures formed in fatigued single crystal copper deformed at $\gamma_{pl} = 2 \times 10^{-3}$ viewed on (111) plane; red and white regions indicate the low- and high-dislocation-density networks, respectively. (b) and (c) Magnified image of the white and red region in (a), respectively.

Chapter 4. Cell structure development during cyclic deformation of near-[001] and near-[011] copper single crystals

In this chapter, we investigated the dislocation structures in near-[001] and near-[011] copper single crystals under high strain amplitudes, with a particular emphasis on the characterization of cell structures. The dislocation structures were observed by scanning electron microscopy electron-channeling contrast (SEM-ECC) and HV-STEM.

As shown in Fig. 3, in the plateau region ($\gamma_{pl} \leq 7.5 \times 10^{-3}$) of near-[011] copper single crystals, the matrix were dislocation walls formed by single-slip. The formation plane of walls is perpendicular to the direction of activated slip system. The (111) cell structures formed in single-slip DBs. After the plateau region ($\gamma_{pl} > 7.5 \times 10^{-3}$), multiple slip systems were activated to form multiple-slip DBs. And the (111) cell structures preferentially formed in multiple-slip DBs, indicating that these DBs can accommodate higher plastic strain compared to the single-slip DBs.

For [001] copper single crystals, the (111) cell structure uniformly formed in the matrix without the formation of DBs. As the cumulative plastic strain increases, ($\bar{1}$11) critical slip plane also activates to form a cell boundary to accommodate higher cumulative plastic strains. In

addition, we used the virtual-STEM technique to analyze the formation mechanism of the (111) cell boundary in [001] and [011] copper crystals and found that, similar to [$\bar{1}$11] crystals, it was formed by the co-activation of the primary and coplanar slip systems.

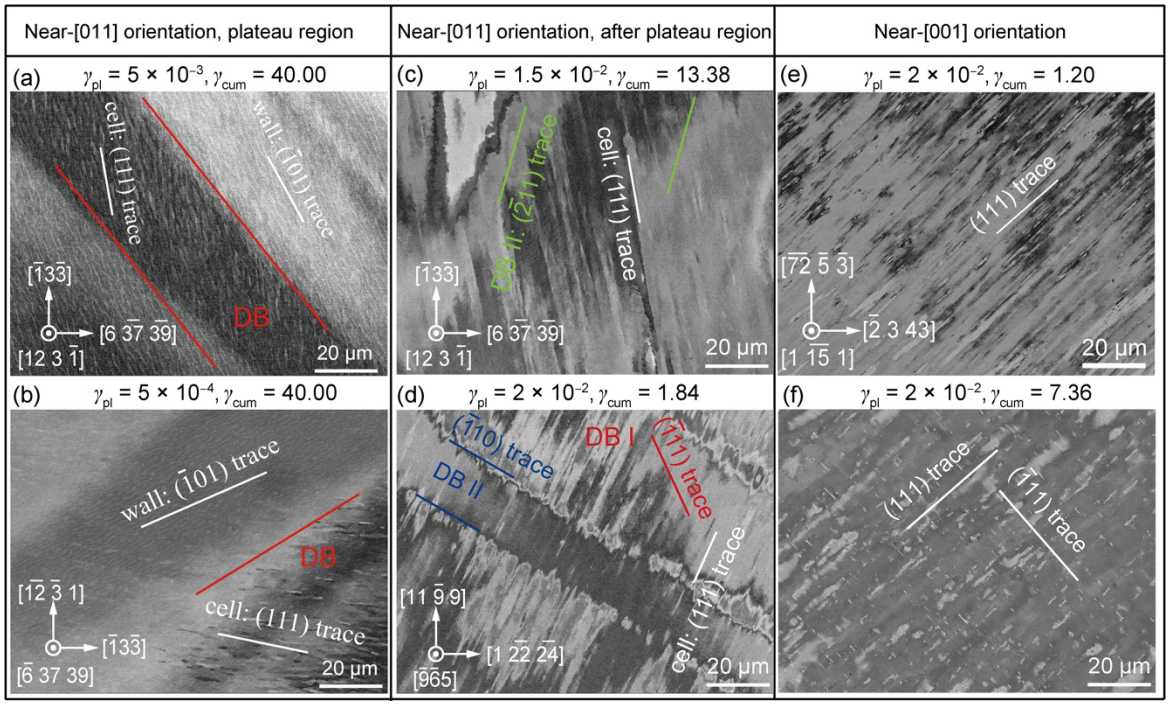

Fig. 3. SEM images of dislocation structures in copper single crystal. (a, b) [011] crystals in the plateau stage ($\gamma_{pl} \leq 7.5 \times 10^{-3}$) observed from the double-plane. (c, d) [011] crystals beyond the plateau stage ($\gamma_{pl} > 7.5 \times 10^{-3}$). (e, f) [001] crystals under $\gamma_{pl} = 2 \times 10^{-2}$: (e) $\gamma_{cum} = 1.20$ and (f) $\gamma_{cum} = 7.36$.

Chapter 5: General conclusions and future perspectives

This chapter summarizes the main findings of the present study and discusses possible future research directions and perspectives.